Quasi-Fermi-level splitting in ideal silicon nanocrystal superlattices

P. Löper,[1,*] R. Müller,[1] D. Hiller,[2] T. Barthel,[3] E. Malguth,[3] S. Janz,[1] J. C. Goldschmidt,[1] M. Hermle,[1] and M. Zacharias[2]
[1]Fraunhofer Institute for Solar Energy Systems (ISE), Heidenhofstraße 2, DE-79110 Freiburg, Germany
[2]University of Freiburg, IMTEK, Nanotechnology, Georges-Köhler-Allee 103, DE-79110 Freiburg, Germany
[3]Helmholtz-Centre Berlin for Materials and Energy, Kekuléstraße 5, DE-12489 Berlin, Germany
(Received 24 August 2011; revised manuscript received 27 October 2011; published 22 November 2011)

Silicon quantum dots open up the possibility for solar cells with a higher voltage than in the Si bulk but still based on crystalline Si. An upper limit of a solar cell's open circuit voltage is the splitting of the quasi-Fermi-levels under illumination. To determine this splitting, the band structure and the density of states of a superlattice of cubic silicon quantum dots is calculated. Furthermore, the absorption and the minority charge-carrier lifetime of size-controlled Si NCs in a silicon dioxide matrix are measured. From these data the excess carrier density under illumination with the AM1.5G solar spectrum is estimated to be about 10^{16} cm^{-3}. Based on the density of states and the carrier concentration, the quasi-Fermi-levels are calculated. Superlattices of silicon nanocrystals in SiO_2, Si_3N_4, and SiC are compared. It is found that under AM1.5G illumination the integrated density of states in the first miniband is always much higher than the excess carrier density and the splitting of the quasi-Fermi-levels follows the calculated band gap with an offset of about 0.36 eV.

DOI: 10.1103/PhysRevB.84.195317 PACS number(s): 88.40.hj, 73.22.−f, 78.67.Bf

I. INTRODUCTION

Silicon nanocrystals (Si NCs) with quantum confined carriers have a band gap which is higher than that of bulk Si and is adjustable through the NC size.[1–3] This opens up the opportunity to create a high band-gap solar cell which can be combined with a bulk Si solar cell to realize a crystalline Si dual junction solar cell. According to calculations by Meillaud *et al.*[4] the 33% Shockley Queisser limit of a solar cell with a 1.12 eV band gap increases to 45% when combined with a 1.7 eV top solar cell.

Quantum confinement in Si NCs and its size dependence has been investigated theoretically[1,5] and proven experimentally by absorption[6] and photoluminescence.[2,4,7] However, for an increased efficiency compared to the single junction bulk cyrstalline Si solar cell, it is not the band gap but the open circuit voltage of the Si NC solar cell that is the decisive parameter. An upper limit for the open circuit voltage is given by the quasi-Fermi-level splitting of the solar cell absorber layer.

In this paper, the quasi-Fermi-level splitting of Si NCs in SiO_2, Si_3N_4, and SiC is calculated based on experimental data of carrier generation and recombination and a theoretical band-structure model.

II. APPROACH

The open circuit voltage of a *pn* or *pin* solar cell having perfect selective contacts can be approximated by the quasi-Fermi-level splitting in the illuminated absorber. The quasi-Fermi energy $E_{F,n}$ is the thermodynamic parameter describing the electron concentration for a given density of states:

$$n = \int N(E) \frac{1}{1 + \exp\left(\frac{E - E_{F,n}}{k_B T}\right)} dE. \quad (1)$$

$N(E)$ is the density of states (per volume) at the energy E, n is the total charge-carrier density of the respective carrier type, k_B denotes Boltzmann's constant, and T is the temperature. The temperature is taken to be 300 K throughout this paper.

In order to determine the quasi-Fermi-levels from Eq. (1), the density of states and the charge-carrier concentration have to be known. For the density-of-states calculation we model the Si NC layer as an ideal cubic superlattice and use the envelope function approach[8] to obtain the dispersion relation $E(\boldsymbol{k})$. The excess charge-carrier concentration Δn is obtained as the product of the carrier generation rate G and the carrier lifetime τ, $\Delta n = G\tau$, which were determined by absorption and transient photoluminescence measurements, respectively. Assuming undoped material, $n_0 \ll \Delta n$ holds and we obtain the charge-carrier density from

$$n \approx \Delta n = G\tau \approx \frac{1}{d} \int A(\lambda) j_\gamma(\lambda) d\lambda\, \tau. \quad (2)$$

$A(\lambda)$ is the absorption of the sample with thickness d and j_γ represents the AM1.5G photon current density. The calculation of the quasi-Fermi-level for holes $E_{F,p}$ is done analogously to the way shown here for electrons.

III. THEORY AND MODELING

To calculate the band structure and the density of states, the nanocrystal system is modeled as a superlattice of periodically arranged cubic quantum dots embedded in a matrix of dielectric material, as shown in Fig. 1. The band-structure calculation follows the works of Jiang *et al.*[9] and Lazarenkova *et al.*[8] Each cube in Fig. 1 represents a nanocrystal of size L, and the space between the cubes is filled with matrix material. The periodicity P is the same along the orthogonal spatial axes x, y, and z so that the distance between the nearest cubes is $S = P - L$.

Because of its higher band gap in comparison to silicon, the dielectric matrix forms a potential barrier for charge carriers. This leads to a periodic array of rectangular potential barriers as introduced by Kronig and Penney. The barrier height V_0 depends on the matrix material and is given in Table I. In agreement with Jiang *et al.*,[9] an effective mass of electrons and holes of 0.4 m_0 is assumed for the matrix, which is a reasonable value for all three dielectric matrix materials. m_0

 ©2011 American Physical Society

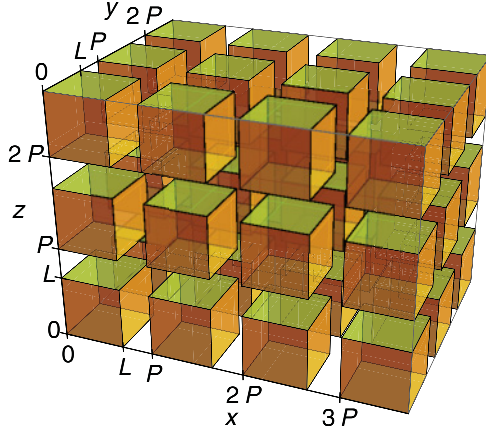

FIG. 1. (Color online) Ideal superlattice of cubic quantum dots with size L and periodicity P along each spatial direction.

is the electron invariant mass. Within the nanocrystals, the effective mass m^* is set to $0.33m_0$ for electrons and $0.28m_0$ for holes, which are the geometric averages of the anisotropic effective masses in bulk silicon.[10]

The charge carriers within the potential are described by the Schrödinger equation

$$\frac{\hbar}{2m^*}\nabla^2\psi(r) + [E - V(r)]\,\psi(r) = 0, \tag{3}$$

with the reduced Planck's constant $\hbar$, effective mass m^*, wave function ψ, position vector $\boldsymbol{r}$ and energy E. For the potential V, the periodic array of rectangular potential barriers has to be inserted. With a further simplification, namely, by separating the spatial directions,[8] the Schrödinger equation is solvable analytically.[11]

These solutions give a relation between the wave vector $\boldsymbol{k}$ and the energy E, resulting in the electronic band structure $E(\boldsymbol{k})$. Figure 2 shows the calculated band structure above the bulk Si band gap for a superlattice of 2 nm silicon quantum dots with 0.5 nm spacing in a Si_3N_4 matrix. Si_3N_4 is chosen to illustrate the energy bands because their structure is well visible. In SiO_2 the energy bands are relatively flat due to the large potential barrier. The energy bands are denoted by their quantum numbers and degeneracy. They range over small energy domains separated by regions without states and are thus called minibands.

The density of states $N(E)$ for electrons in the superlattice is given by an integral over the surface A:[12]

$$N(E) = \frac{2}{(2\pi)^3}\oint_S \frac{dA}{\nabla E(\boldsymbol{k})}, \tag{4}$$

TABLE I. Barrier height V_0 for electrons and holes in the modeled superlattice for the three prominent matrix materials SiC, Si_3N_4, and SiO_2.[9]

	SiC	Si_3N_4	SiO_2
Barrier height for electrons (eV)	0.5	1.9	3.2
Barrier height for holes (eV)	0.9	2.3	4.7

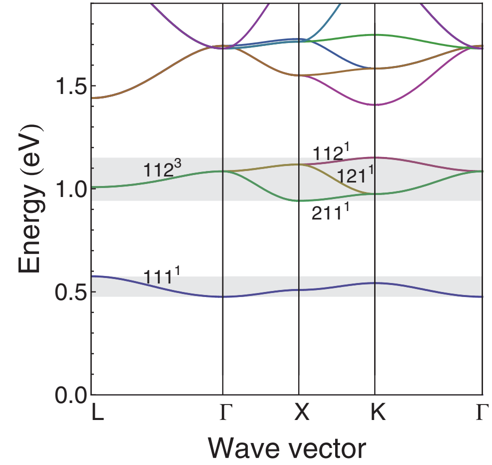

FIG. 2. (Color online) Band structure calculated for 2 nm silicon quantum dots with a distance of 0.5 nm embedded in a silicon nitride matrix. The conduction-band edge of bulk silicon is set as the reference point for the energy axis with $E = 0$.

evaluated in the first Brillouin zone. In this work, the integral was computed by a finite element method[13] dividing the first Brillouin zone into 24 576 tetrahedrons. In each tetrahedron a linear function was used to approximate the band structure $E(\boldsymbol{k})$.

IV. EXPERIMENTAL

Si NCs in SiO_2 were fabricated on synthetic quartz glass (Suprasil 1) by thermal evaporation of SiO powder under high vacuum ($SiO_{x=1.2}$) or in a controlled oxygen ambient (SiO_2). Thereby, a superlattice (SL) structure with 50 bilayers was deposited with each bilayer consisting of a 3 nm SiO_2 barrier and a Si-rich oxide (SRO) layer of 2, 4, and 6 nm for the three samples, respectively. All samples were capped with a 10 nm SiO_2 layer. The samples were annealed for 1 h at 1100 °C in Ar atmosphere to induce Si NC formation. Afterwards, the samples were annealed in forming gas at 420 °C for 20 min to passivate defects at the Si NC surface. Structural characterization including high-resolution transmission electron micrographs can be found in Ref. 14. The approximate crystallite sizes according to these former studies are 2, 3.5, and 5 nm. The samples are labeled S2, S3.5, and S5 throughout this paper. Reflection R and transmission T spectra were measured using a Varian Cary 500i spectrophotometer equipped with an integrating sphere. The absorption A was calculated as $A = 1-R-T$.

Time-resolved photoluminescence was measured at room temperature. A pulsed nitrogen gas laser operating at 337 nm with 3 nm pulse width and a repetition rate below 10 Hz was used for excitation. The energy/pulse on the sample was 70 μJ on a spot of $\sim$0.6 cm^2. The luminescence was detected with a prism monochromator and a silicon avalanche photodiode. The transient was measured in a spectral window of 70 nm around the maximum steady-state photoluminescence intensity with a time resolution of the overall system better than 300 ns.

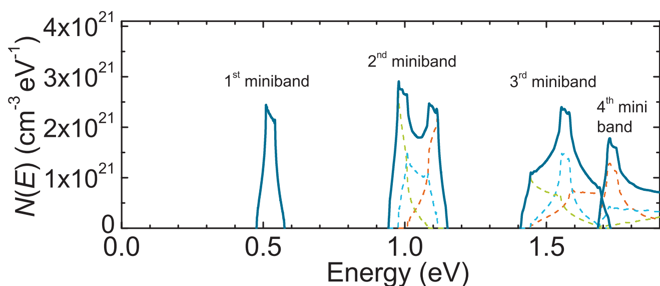

FIG. 3. (Color online) Density of states calculated for 2 nm silicon quantum dots with a distance of 0.5 nm embedded in a silicon nitride matrix. The origin of the energy axis equals the conduction-band edge of bulk silicon.

V. RESULTS AND DISCUSSION

A. Density of states and quasi-Fermi-level

The density of states for different superlattices and geometries was calculated to investigate the influence of the dot size, interdot distance, and matrix material.

Figure 3 shows the calculated density of states above the band gap for 2 nm silicon quantum dots with 0.5 nm spacing in a Si_3N_4 matrix. The dashed lines represent the contribution of the single energy bands whereas the full lines and filled areas stand for the complete minibands. The dot size mainly affects the position of the minibands in the energy diagram, depicted in Fig. 4(a) for a SiO_2 matrix. The variation of the Si quantum dot size with a distance of 0.5 nm shows a strong shift in position of the first miniband toward higher energies for smaller quantum dots. The quantum dot size also affects the width of the miniband. However, this feature is much more strongly influenced by the interdot distance. As shown in Fig. 4(b), a reduction of the interdot distance from 1 to 0.25 nm successively changes the shape of the first miniband from a narrow needle to wider distribution. Additionally, the position of the miniband is slightly shifted toward lower energies.

The band gap of the matrix material influences both the position and the width of the minibands. Figure 4(c) shows the situation for the three technologically relevant matrices SiC, Si_3N_4, and SiO_2. A high barrier for charge carriers, like that in a SiO_2 matrix (see Table I), results in strong quantum confinement. The first miniband is far away from the bulk silicon conduction-band edge, and is narrow in comparison with silicon quantum dots in matrices with lower barriers. A different matrix material [Fig. 4(c)] changes the miniband shape (width and height) and position but leaves the area under it constant because the total number of electronic states remains the same.

In summary, the density of states in the modeled superlattice can be controlled by a set of three parameters, namely, the size of the quantum dots, the interdot distance, and the matrix material. The kind of matrix material has no influence on the integrated density of states in the respective miniband. However, the dot size and the interdot distance do have such an influence, as the number of states per unit volume depends on the Si NC volume concentration. For reasonable dot sizes between 1.5 and 5 nm and distances between 0.5 and 4 nm, the integrated density of states of the first miniband N_1 is between 10^{18} and 10^{21} cm^{-3} (see Fig. 5).

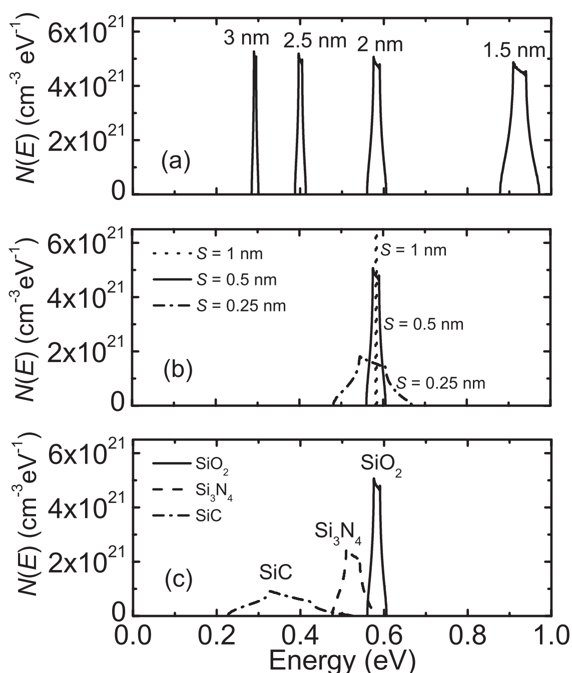

FIG. 4. Calculated density of states in the first miniband above the Si band gap for a superlattice of Si quantum dots in SiO_2, Si_3N_4, and SiC. (a) Size variation for 0.5 nm separated Si quantum dots in SiO_2. (b) Distance variation for 2 nm Si quantum dots in SiO_2. (c) 2 nm Si quantum dots with 0.5 nm spacing in various matrices.

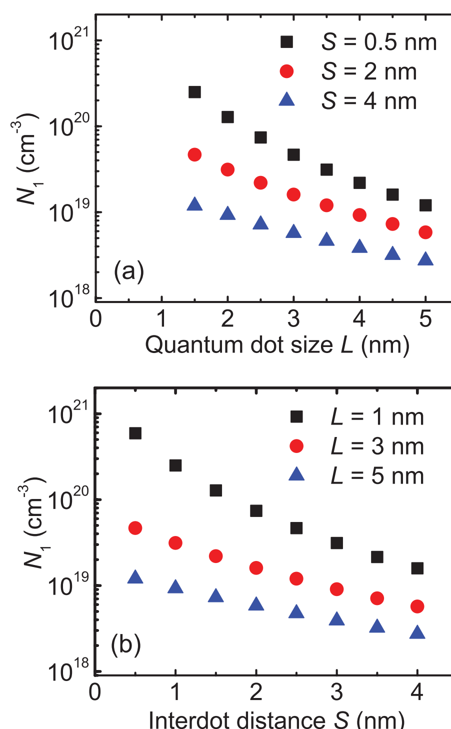

FIG. 5. (Color online) Calculated density of states in the first mini N_1 band above the band gap for silicon quantum dots in SiO_2. (a) Variation of the quantum dot size. (b) Variation of the quantum dot distance.

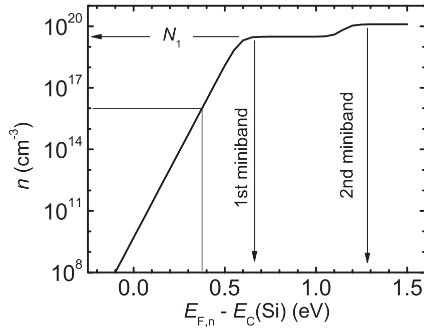

FIG. 6. Relation between the carrier concentration n and the quasi-Fermi-level for electrons $E_{F,n}$ for 2 nm silicon quantum dots with 2 nm spacing in SiO_2. When the first miniband is full ($n = N_1$), the quasi-Fermi-level rises towards the second miniband. The thin lines indicate the quasi-Fermi-level for a carrier density of 10^{16} cm^{-3}.

The presented calculation of the density of states was done in order to obtain a relation between the concentration n and the quasi-Fermi-level of one charge-carrier type, given by Eq. (1). Figure 6 illustrates this relation for electrons in the case of 2 nm quantum dots with 0.5 nm spacing in SiO_2. For n much smaller than the density of states in the first miniband N_1, n rises logarithmically with $E_{F,n}$ because the Fermi-Dirac distribution shifts to higher energies, Eq. (1). Once the first miniband is filled and the second miniband starts to be populated, $E_{F,n}$ jumps toward the latter. The effects for holes and the corresponding quasi-Fermi-level $E_{F,p}$ are analogous and not discussed here.

B. Excess carrier density

In order to get a realistic value for the excess carrier concentration Δn, the spectrally resolved optical absorption A and the luminescent lifetime was measured for a set of samples with silicon nanocrystals in a SiO_2 matrix with approximate crystallite sizes of 2, 3.5, and 5 nm. The experimental data reported in this paper, carried out to determine the excess carrier density in Si NC, are exclusively related to a matrix of SiO_2, which is known to present the best properties. Figure 7 shows the absorption data and the AM1.5G solar spectrum. For simplicity, optical effects such as multiple reflections were neglected. We assumed that every absorbed photon with a wavelength λ smaller than 600 nm creates one electron-hole pair and calculated the excess carrier concentration Δn from Eq. (2). Other effects like the generation of multiple excitons per absorbed photon are neglected here.

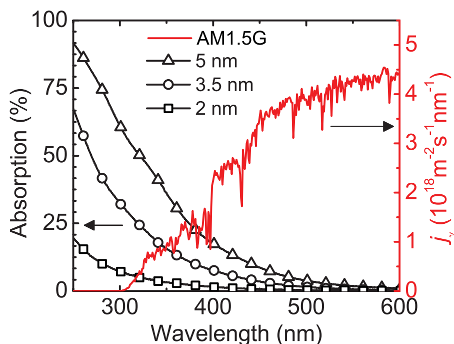

FIG. 7. (Color online) Spectral absorption of three samples each containing 50 bilayers of silicon nanocrystals (different sizes: 2, 3.5, and 5 nm) in a SiO_2 matrix (lines with symbols) and the AM1.5G solar spectrum (continuous line).

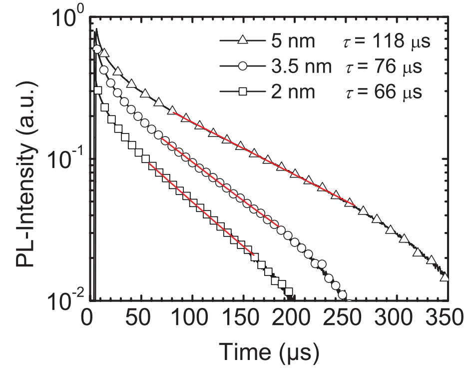

FIG. 8. (Color online) Photoluminescence decay of Si NC in SiO_2 with approximate sizes of 2, 3.5, and 5 nm. The lifetime was obtained from a single-exponential fit to the data (continuous lines).

Time-resolved photoluminescence for the same Si NC sizes (2, 3.5, and 5 nm) is shown in Fig. 8. The luminescence lifetime was obtained by a single-exponential fit (continuous line in Fig. 8). The origin of Si NC photoluminescence has been intensively discussed in recent years. In his comprehensive review, Sa'ar[15] elucidated the effects of surface chemistry and quantum confinement. Godefroo *et al.*[2] demonstrated how the origin of the photoluminescence (PL) from Si NC in SiO_2 can be switched from defect related to quantum confined by a hydrogen treatment. In order to record band-band luminescence but not that of trapped carriers at surface states, the Si NC samples used in this work were passivated in forming gas after the high-temperature annealing step (see Sec. IV). The dependence of the lifetime on Si NC size (Fig. 8) supports the hypothesis that the luminescence stems from quantum confined carriers rather than from localized surface states. Lifetime values between 66 and 118 μs were measured, which is in very good agreement with other measurements.[6] The resulting excess charge-carrier density lies between 0.15×10^{16} cm^{-3} for the S2 sample and 1.66×10^{16} cm^{-3} for the S5 sample (see Table II). The excess carrier concentration correlates with the size of the nanocrystals. The bigger the nanocrystals, the stronger their absorption is, especially in the visible range, in which the solar photon flux is increasingly intense. Apart from that, Δn is always significantly smaller than the integral density of states in the first miniband (cf. Fig. 5). Hence, it is clear that the quasi-Fermi-levels lie between the first miniband above and the first miniband below the band gap.

TABLE II. Estimated excess carrier concentration Δn in different NC samples under illumination with the AM1.5G solar spectrum. Approximate NC sizes are 2, 3.5, and 5 nm.

	S2	S3.5	S5
Δn (cm^{-3})	0.15×10^{16}	0.65×10^{16}	1.66×10^{16}

C. Quasi-Fermi-level splitting

This work aims at obtaining a conservative estimate for the quasi-Fermi-level splitting within Si NC superlattices. As can be seen in Fig. 6, the quasi-Fermi-level depends roughly logarithmically on Δn. Because the dependence on the position of the first miniband and its density of states [overlap integral in Eq. (1)] is much more prominent, we neglect effects of the charge-carrier density for further discussion and set it to a fixed value of 10^{16} cm^{-3}.

For 2 nm NCs in SiO_2 with 2 nm spacing, Eq. (1) with $n \approx \Delta n = 10^{16}$ cm^{-3} yields a quasi-Fermi-level for electrons $E_{F,n}$ of about 0.375 eV above the conduction-band edge of bulk silicon. This is also illustrated in Fig. 6 (thin black lines). $E_{F,p}$ is determined in the same way (not shown here) and lies in this case about 0.495 eV below the valence-band edge of bulk silicon. The splitting of the quasi-Fermi-levels ΔE_F then results in

$$\Delta E_F = E_{F,n} - E_{F,p} = E_{G,\mathrm{Si}} + 0.375\ \mathrm{eV} + 0.495\ \mathrm{eV}, \qquad (5)$$

with the band gap of bulk silicon $E_{G,\mathrm{Si}} = 1.12$ eV.

The density of states was calculated for different superlattices with varying size and distance of the quantum dots in SiC, Si_3N_4, and SiO_2 matrices. Subsequently, the splitting of the quasi-Fermi-levels was calculated for every considered NC size with $\Delta n = 10^{16}$ cm^{-3}, and for 10^{14} and 10^{18} cm^{-3} as a simple parameter variation. Figure 9 shows the results. For all three matrices, the band gap strongly depends on the quantum dot size. The smaller the dots, the stronger the quantum confinement, and therefore the larger is the band gap. This effect is especially pronounced for very small quantum dots. The offset between ΔE_F and the band gap depends only slightly on the dot size, the interdot distance, and the matrix material. The offset increases from 0.33 eV for 5 nm dots to 0.44 eV for 1.5 nm dots for one sun illumination. The observation that ΔE_F mainly follows the band gap can be explained with the integrated density of states in the first miniband N_1, which is always several orders of magnitude higher than the excess carrier concentration Δn and the fact that the first miniband is very narrow. Figure 9 also shows how the quasi-Fermi-level splitting depends on the charge-carrier concentration. A higher charge-carrier concentration can be achieved by means of light trapping[16] or an increased lifetime. A 100-fold higher carrier concentration would increase the quasi-Fermi-level splitting by 0.24 eV.

The procedure presented here involves several simplifications and relies on the idealized case of a cubic superlattice with monodisperse NCs. To check consistency with other band-gap-related data, we compare in Fig. 10 the quasi-Fermi-level splitting with the measured optical absorption gap E_{03} and the position of the photoluminescence maximum E_{PL}. The three values show similar size dependence and the same sequence except for the smallest NC size (2 nm). However, bearing in mind the severe simplifications made (cubic shape, perfect size distribution, etc.), the discrepancy for very small NCs is no surprise. For sizes larger than approximately 2.5 nm, the calculation of the quasi-Fermi-level splitting seems to be reasonable.

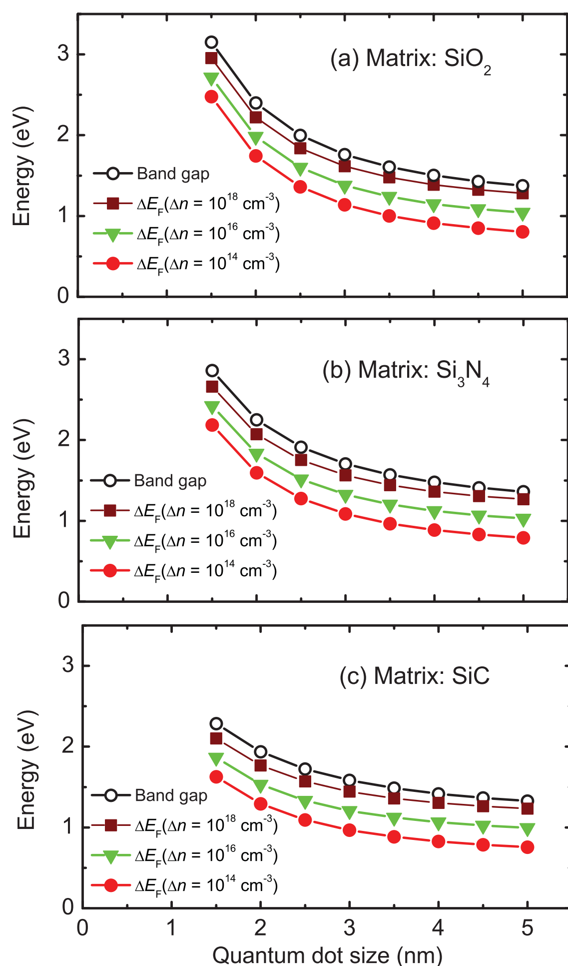

FIG. 9. (Color online) Calculated band gap (black) and splitting of the quasi-Fermi levels ΔE_F for silicon quantum dots in a SiO_2 (a), Si_3N_4 (b), and SiC (c) matrix, all with an interdot distance of 2 nm. Illumination with one sun corresponds to $\Delta n = 10^{16}$ cm^{-3}.

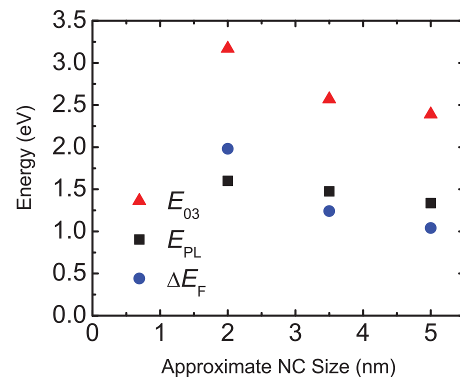

FIG. 10. (Color online) Experimental values of the photoluminescence maximum E_{PL} and the optical gap E_{03} of Si NCs in SiO_2 in comparison with the calculated quasi-Fermi-level splitting.

VI. CONCLUSION

The quasi-Fermi-level splitting of Si NC superlattices in SiO_2, Si_3N_4, and SiC was investigated using the envelope function approximation to calculate the energy-band structure and the density of states together with experimental values of the charge-carrier density. To estimate the charge-carrier

density, absorption and carrier lifetime measurements were performed on size-controlled Si NCs in SiO_2 with sizes of 2, 3.5, and 5 nm. Based on these measurements, the carrier density is estimated to 10^{16} cm^{-3} at 1 sun illumination. In this case, the quasi-Fermi-level splitting was shown to follow the band gap with an offset of approximately 0.36 eV. A 100-fold higher carrier generation enhances the quasi-Fermi-level splitting by 0.24 eV. Given a sufficiently high short circuit current and fill factor, this would allow a significantly higher efficiency to be attained.

ACKNOWLEDGMENTS

The authors would like to thank G. H. Bauer and F. Voigt for valuable discussion and measurements. The research leading to these results has received funding from the European Community's Seventh Framework Programme (FP7/2007-2013) under grant agreement No. 245977. P.L. gratefully acknowledges scholarship support from the Reiner Lemoine Stiftung, and ideational support from the Heinrich Böll Stiftung.

*Philipp.Loeper@ise.fraunhofer.de

[1] C. Delerue, G. Allan, and M. Lannoo, Phys. Rev. B **48**, 11024 (1993).
[2] S. Godefroo, M. Hayne, M. Jivanescu, A. Stesmans, M. Zacharias, O. I. Lebedev, G. Van Tendeloo, and V. V. Moshchalkov, Nature Nanotechnol. **3**, 174 (2008).
[3] M. Zacharias, J. Heitmann, R. Scholz, U. Kahler, M. Schmidt, and J. Bläsing, Appl. Phys. Lett. **80**, 661 (2002).
[4] F. Meillaud, A. Shah, C. Droz, E. Vallat-Sauvain, and C. Miazza, Sol. Energy Mater. Sol. Cells **90**, 2952 (2006).
[5] T. Takagahara and K. Takeda, Phys. Rev. B **46**, 15578 (1992).
[6] D. Kovalev, J. Diener, H. Heckler, G. Polisski, N. Künzner, and F. Koch, Phys. Rev. B **61**, 4485 (2000).
[7] J. Heitmann, F. Müller, L. Yi, M. Zacharias, D. Kovalev, and F. Eichhorn, Phys. Rev. B **69**, 195309 (2004).
[8] O. L. Lazarenkova and A. A. Balandin, J. Appl. Phys. **89**, 5509 (2001).
[9] C.-W. Jiang and M. A. Green, J. Appl. Phys. **99**, 114902 (2006).
[10] S. M. Sze, *Semiconductor Devices, Physics and Technology*, 2nd ed. (Wiley, Hoboken, NJ, 2001).
[11] G. Bastard, Phys. Rev. B **24**, 5693 (1981).
[12] N. W. Ashcroft and N. D. Mermin, *Solid State Physics* (Holt-Saunders, Tokyo, 1976).
[13] G. Lehmann and M. Taut, Phys. Status Solidi B **54**, 469 (1972).
[14] D. Hiller, S. Goetze, F. Munnik, M. Jivanescu, J. W. Gerlach, J. Vogt, E. Pippel, N. Zakharov, A. Stesmans, and M. Zacharias, Phys. Rev. B **82**, 195401 (2010).
[15] A. Saar, J. Nanophotonics **3**, 032501 (2009).
[16] E. Yablonovitch and G. D. Cody, IEEE Trans. Electron Devices **29**, 300 (1982).